RASĀYAN *J. Chem.*
Vol. 19 | No. 3 | 1331-1339 | July-September | 2026
ISSN: 0974-1496 | e-ISSN: 0976-0083 | CODEN: RJCABP
http://www.rasayanjournal.com
http://www.rasayanjournal.co.in

DISCOVERY OF POTENTIAL ALDOSED REDUCTASE (ALR2) INHIBITORS FROM DIHYDROPYRIMIDINONE DERIVATIVES: AN *In-silico* STUDY

H. Suwito[1,✉], M.F.B. Darmawan [1], K.U. Haq[1,2], and I. Siswanto[1]
[1]Department of Chemistry, Faculty of Science and Technology, Universitas Airlangga, Surabaya-60115,Indonesia
[2]University of CoE-Research Center for Bio-Molecule Engineering (BIOME), Universitas Airlangga, Surabaya-60115, Indonesia
✉Corresponding author: hery-s@fst.unair.ac.id

ABSTRACT
Aldose reductase 2 (ALR2) plays a central role in the pathogenesis of diabetic complications, including neuropathy, nephropathy, and retinopathy, yet the clinical translation of ALR2 inhibitors remains limited by suboptimal efficacy and pharmacokinetic profiles. In this study, a comprehensive in silico strategy was employed to design and evaluate dihydropyrimidinone (DHPM) derivatives as novel ALR2 inhibitors. A virtual library of 288 DHPM compounds was constructed and screened using molecular docking, identifying 87 candidates with binding affinities and interaction patterns comparable to the reference ligand M15. Subsequent ADMET and drug-likeness filtering refined these to three lead compounds—DU18 (2-(5-(methoxycarbonyl)-2-oxo-6-(4-(trifluoromethyl)phenyl)-1,2,3,6-tetrahy-dropy-rimidin-4-yl)acetate), DT12 (2-(5-(methoxycarbonyl)-6-(4-methoxyphenyl)-2-thioxo-1,2,3,6-tetrahydro-pyri-midin-4-yl)acetate), and DT18(2-(5-(methoxycarbonyl)-2-thioxo-6-(4-(trifluoro-methyl)phenyl)-1,2,3,6-tetrahydropyrimi-din-4-yl)acetate)—exhibiting favorable pharmacokinetic and toxicity profiles aligned with established ALR2 inhibitors. Molecular dynamics simulations confirmed the stability of these ligands within the ALR2 active site, highlighting persistent interactions with key catalytic residues. Their predicted binding energies suggest inhibitory potential comparable to zopolrestat. Beyond identifying promising candidates, this work contributes a rational design framework integrating structure-based screening, pharmacokinetic filtering, and dynamic validation to address key limitations in ALR2 inhibitor development. The findings expand the chemical space of DHPM-based scaffolds and provide mechanistic insights into ligand–enzyme interactions critical for potency and selectivity. These results offer a foundation for future experimental validation and optimisation, supporting the development of more effective therapeutics for diabetic complications and demonstrating the value of computational approaches in accelerating early-stage drug discovery.
Keywords: Diabetes Mellitus, Dihydropyrimidinone Derivatives, ALR2 Inhibitor, Molecular Docking, Molecular Dynamic Simulation

RASĀYAN *J. Chem.*, Vol. 19, No.3, 2026

INTRODUCTION

Diabetes mellitus is a chronic metabolic condition characterised by persistently elevated blood glucose levels caused by impaired insulin secretion, reduced insulin effectiveness, or a combination of both, and it will increase about 45% by the end of 2050.[2] Although various antidiabetic medications are widely available on the market, but drugs to combat the diabetes mellitus complications, such as retinopathy, nephropathy, and neuropathy are still in demand. Furthermore, some other complications, such as ketoacidosis, reduced immunity, hyperosmolar to pneumonias, are also observed.[3] Tolrestat and zenarestat exhibited some benefits against diabetic neuropathy, but concerns about liver toxicity leading to withdrawal from use in humans for tolrestat and impaired kidney function for zenarestat.[1] Related to diabetic complications, the role of aldose reductase (ALR2) in within the polyol pathway of glucose metabolism is well known. The polyol pathway involves a two-step process in the conversion of glucose to fructose, that are the conversion of glucose through reduction to sorbitol catalyzed by aldose reductase in the involvement of NADPH, followed in the second step is the enzymatic transformation of sorbitol to fructose using NAD^+ as a coenzyme.[5] Therefore, designing inhibitor of aldose reductase (ALR2) is

http://doi.org/10.31788/RJC.2026.1939735

considered as the key therapeutic strategy to fight diabetes complications.[4] In hyperglycemia circumstances, as in diabetes, the polyol pathway increases activity. Consequently, proceed accumulation of sorbitol resulted in cellular and organ injury. In the case of excessive accumulation of sorbitol, decreasing myoinositol in the peripheral nerves takes place, which resulted decreasing in Na^+ or K^+-ATPase activity, which is essential for nerve conduction. Briefly, increasing polyol activity and over-utilisation of NADPH by aldose reductase can cause the compromise of several other homeostatic mechanisms. On the other hand, the depletion of NADPH resulted in a decrease in both nitric oxide and glutathione production. Declining nitric oxide production causes a decrease in vasodilation as observed in circulatory abnormalities, while the decline in glutathione production causes an elevation of reactive oxygen species that leads to impaired endothelial cell function.[6] Although complications of diabetic neuropathy are commonly observed in diabetes, their precise underlying mechanisms remain incompletely understood, which contributes to the lack of curative therapies for this condition. Currently, pharmacological agents prescribed for diabetic neuropathy are largely empirical and focus only on symptomatic relief rather than disease modification. Consequently, existing research has been directed toward the development of agents that inhibit the activity of aldose reductase (ALR2) in order to reduce sorbitol accumulation. Moreover, it has been proposed that oxidative stress and osmotic stress induced by activation within the polyol pathway act synergistically in the aetiology of diabetic cataract.[7] Based on the chemical structure, ALR2 inhibitors are categorised into three groups, namely acetic acid compounds, spiro-hydantoins, and succinimides. In recent decades, these inhibitors can be obtained from both natural and synthetic sources.[8] However, a drug exhibiting low adverse effects and efficient inhibition activity is still in demand.[9] In this article, we report the design and discovery of ALR2 inhibitors based on dihydropyrimidinone (DHPM) derivatives. DHPM is a product of Biginelli's reaction, a one-pot multi-component reaction consisting of the β-diketo compound, urea or thiourea, and derivatives of benzaldehyde[10] employing an in-silico study. DHPM scaffold is versatile to be modified to achieve a similar structure with already known ALR2 inhibitors.[11] This in silico study supports the United Nations Sustainable Development Goals (SDGs) by promoting sustainable and resource-efficient research practices through the reduction of laboratory waste, decreased energy consumption, and minimised reliance on experimental materials and animal testing, particularly contributing to SDG 3, 9,12, and 13. In this paper, we used acetic-based DHPM derivatives as the research objects. Based on the literature search, there are no articles that reported DHPM derivatives as ALR2 inhibitors.

EXPERIMENTAL

Materials

Three-dimensional crystal structure of human aldose reductase-2 (ALR2) complexed with the ligand M15 (5-chloro-2-(2-fluoro-4-iodobenzyl)carbamoyl)phenoxyacetic acid) was obtained from the RCSB Protein Data Bank (PDB ID: 4LB3).[12] A total of 288 designed DHPM derivatives were used as candidates, while 18 already marketed ALR2 inhibitors were used as comparative compounds.

Preparation of ALR-2 Inhibitor Candidates

First, the 3D structures of the candidate inhibitors were generated and protonated at pH 7.4 using Avogadro[12], followed by structural optimisation with Gaussian 16[13] employing the PM7 semi-empirical method. Subsequently, charges were assigned to the candidate compounds using the AM1-BCC method through the antechamber program.[14]

Virtual Screening

Virtual screening was initiated through validation of the docking parameters. The structure of the ligand-protein complex was prepared using the DockPrep module in Chimera.[15] Protein charges were assigned with the ff14SB force field[16], while non-protein components were treated using the AM1-BCC method.[14] A receptor surface excluding hydrogen atom was generated and used to define spheres for docking[17], which were chosen within a 6.0 Å radius of the ligand. Finally, a simulation box with a 7.0 Å radius was constructed for docking calculations. The grid was generated using a Lennard–Jones potential with attraction and repulsion exponents of 6–9.[18] The native ligand was then redocked into the receptor using flexible docking in DOCK6, and successful pose reproduction was confirmed by an RMSD ≤ 2.0 Å.[19]

The validated docking parameters were subsequently applied to virtual screening, and ligands were prioritised for experimental evaluation based on their grid scores and binding conformations.

ADMET Analysis and Selection of Candidates

ADME properties were estimated using the SwissADME web server[20], while poisonousness was evaluated with the TEST program.[20-1] Compounds were advanced based on predefined Selection Score[21] criteria incorporating ADMET parameters and docking grid scores. ADME assessment followed the Lipinski and Ghose–Veber rules[20], considering key physicochemical properties, whereas toxicity evaluation included Ames mutagenicity (M) and LD_{50}. Compounds with Selection Scores (SS) higher than that of the reference drug tolrestat were chosen for molecular dynamics simulations.

Molecular Dynamic Simulation

Molecular dynamics simulations were performed to examine ligand–receptor interactions under physiologically relevant conditions. Three DHPM candidates, along with ligand M15 and zopolrestat, were simulated in complex with ALR-2 using the AMBER software package.[22] The protein was modelled using the FF14SB force field, while the inhibitors were parameterized using the GAFF force field. Each complex was placed in a TIP3P water box with a 10 Å buffer and neutralized by adding Na^+ ions. Energy minimization was carried out using the steepest descent and conjugate gradient methods in three stages with the Sander module of AMBER. Initially, solvent molecules were minimized under positional restraints on the protein termini, followed by minimisation of solvent and side chains with restraints on active-site and terminal residues. Finally, the whole system underwent unrestrained minimization to ensure complete relaxation. It was then gradually heated from 0 to 310 K using the NVT ensemble, followed by equilibration of the system density at 310 K. Subsequent equilibration was performed under NPT conditions through multiple stages with progressively reduced positional restraints on active-site and terminal residues. A 150 ns production MD simulation was then conducted to evaluate system stability, using the sander module of AMBER.

Calculation of the Binding Free Energy

The binding affinity was determined by computing the binding free energy from the last 10 ns of the simulation using 2000 snapshots. Free energy calculations were conducted using the MM-PBSA and MM-GBSA[23] approaches.

$$\Delta G_{bind} = G_{com} - (G_{rec} + G_{lig}) \quad (1)$$

$$\Delta G_{bind} = \Delta H - T\Delta S \approx \Delta E_{MM} + \Delta G_{sol} - T\Delta S \quad (2)$$

$$\Delta E_{MM} = \Delta E_{int} + \Delta E_{ele} + \Delta E_{vdw} \quad (3)$$

$$\Delta G_{sol} = \Delta G_{GB/PB} + \Delta G_{SA} \quad (4)$$

Here, G_{com}, G_{rec}, and G_{lig} represent the free energies of the complex, receptor, and ligand, respectively. The binding free energy is composed of gas-phase enthalpy, solvation free energy, and conformational entropy contributions. The gas-phase term comprises internal, electrostatic, and van der Waals energies, while solvation free energy includes polar and nonpolar contributions calculated using the PB and GB methods in AMBER. An external dielectric constant of 80 and an internal dielectric constant of 1 were applied.

An external dielectric constant of 80 and an internal dielectric constant of 1 were applied. Nonpolar desolvation energy was estimated from SASA using the LCPO method with a 1.4 Å probe, while conformational entropy was omitted because of its high computational demand and relatively low accuracy. Per-residue energy decomposition was carried out using MM-PBSA and MM-GBSA in AMBER, separating the contributions into van der Waals, electrostatic, polar solvation, and nonpolar solvation components.

Trajectory Analysis

Ligand–protein stability was evaluated by analyzing RMSF, radius of gyration, and SASA over 2000 frames from the final 10 ns of the MD simulation.

RESULTS AND DISCUSSION

Design of Target Molecules and Molecular Docking

ALR-2 inhibitors typically feature a carboxylic acid and an aromatic ring, facilitating hydrogen bonding with hydrophilic active-site residues and hydrophobic interactions, including van der Waals and π-π stacking, respectively. In this research, DHPM derivatives containing a carboxylic acid—commonly synthesized via the one-pot Biginelli reaction—served as the molecular scaffold. A set of 288 derivatives was generated by varying benzaldehyde, 1,3-dicarbonyl, and urea/thiourea components, with the core DHPM structure and substitutions summarized in Table-1.

Table-1: Variation of Components for DHPM Candidates: (a) Benzaldehyde, (b) 1,3-dicarbonyl, (c) Urea/Thiourea, and (d) the Core Structure of DHPM Candidates

Component variation			Main core candidates
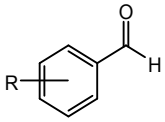 (a)	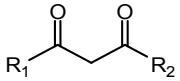 (b)	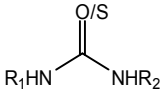 (c)	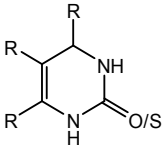 (d)

Validation of Molecular Docking

The crystal structure of the target protein complexed with the reference ligand M15 (PDB ID: 4LB3) was used in this study. Redocking of the ligand confirmed the reliability of the docking parameters, producing a grid score of –69.44 kcal/mol and a DockRMSD of 0.448 Å, which is well under the 2 Å cutoff. This confirmed the reliability of the docking protocol for subsequent experiments. Figure-1 shows a 3D superimposition of the native ligand (brown) and the docked ligand (light blue).

(a) (b)

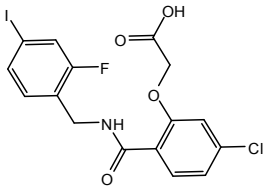

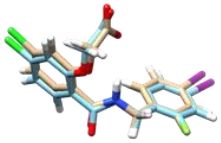

Fig.-1: (a) Structure of Ligand M15; (b) 3D Visualisation of the Superimposed Ligand Pose of the Original (brown) and Re-Docked (light blue) at the Binding Site of 4LB3 Receptor

Analysis of the 4LB3 receptor–M15 complex showed that M15 formed hydrogen bonds with His111 and Trp112, alongside a π-π stacking interaction with Trp112, as depicted in Fig.-2.

(a) (b)

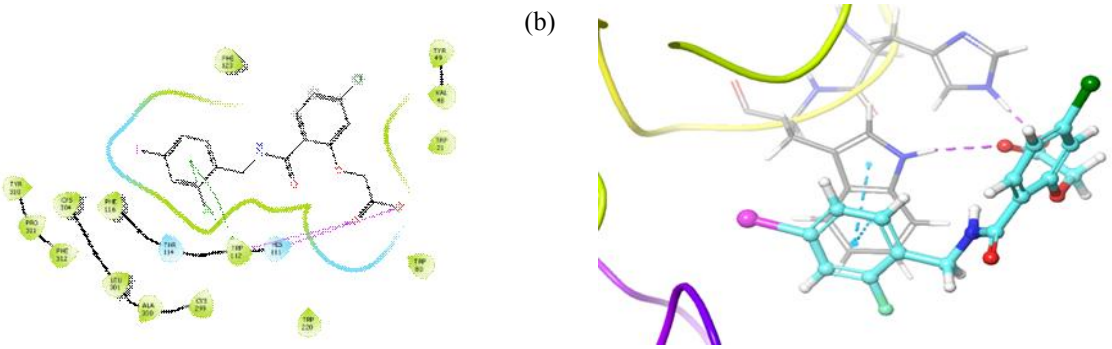

Fig.-2: Interaction Visualization between Ligand M15 and 4LB3 Receptor. (a) 2D; (b) 3D

Docking of 288 DHPM candidates identified 87 with poses similar to M15, showing grid scores from –73.54 to –49.33 kcal/mol. Candidate SDZ28 ranked highest (–73.54 kcal/mol), forming both hydrogen bonds and π-π stacking interactions with Trp112.

ADMET and Drug-Likeness Analysis

The 87 selected candidates were evaluated for ADMET properties and drug-likeness using SwissADME, compared with M15, 17 known ALR-2 inhibitors, and tolrestat as the reference. Candidates with a Selection Score (SS) above that of tolrestat—calculated from grid scores and ADMET parameters—were prioritized. ADME was assessed according to Lipinski, Ghose, and Veber rules, while toxicity was evaluated via Ames mutagenicity and LD_{50} using TEST. Twenty-two candidates exceeded tolrestat in SS, as shown in Fig.-3.

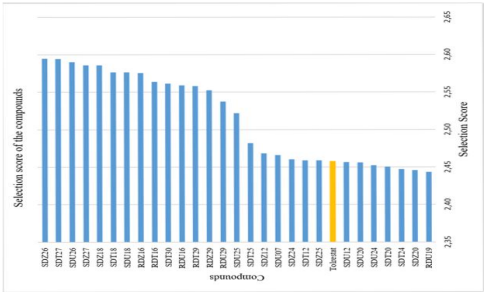

Fig.-3: Graph of SS Analysis of the Selected Candidates and Tolrestat. (yellow bar)

Molecular Dynamic Simulation

Assessment of Stability and Structural Flexibility

Molecular dynamics simulations were performed for 150 ns to evaluate the stability, flexibility, and dynamic behavior of ALR2 and its complexes (ALR2-M15, ALR2-ZST, ALR2-SDU18, ALR2-SDT18, and ALR2-SDT12) using RMSD, RMSF, RoG, and SASA. Backbone RMSD indicated that all systems reached stability (≤0.2 nm; Fig.-4, Table-2), with ALR2-SDT18 showing the highest RMSD (0.171 ± 0.024 nm) and ALR2-ZST the lowest (0.132 ± 0.014 nm), suggesting that ALR2-SDT18 was more dynamic and less stable.

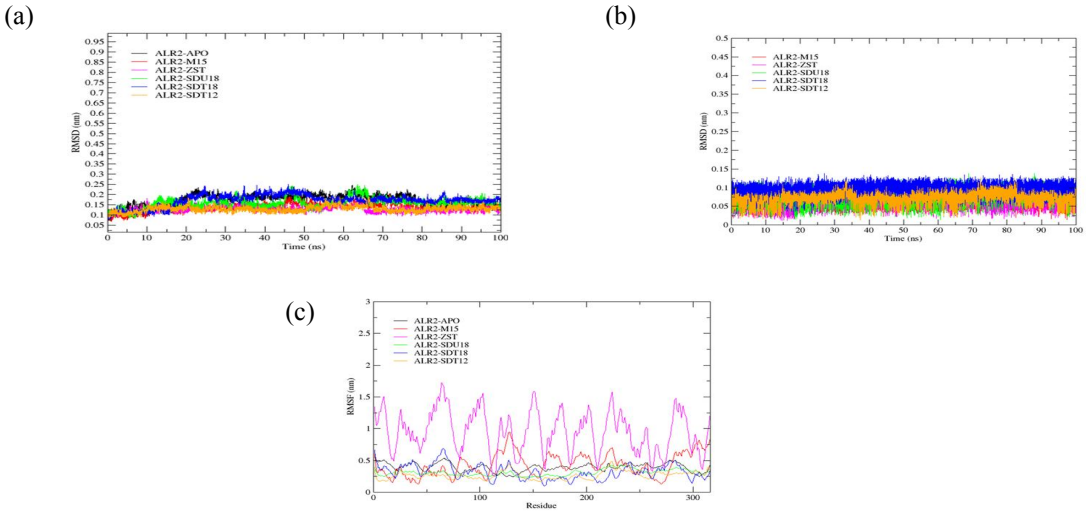

Fig.-4: RMSD Stability During Simulation (a) Backbone, (b) Ligand, (c) RMSF of Flexibility Simulation Results

Table-2: Average RMSD and RMSF Values During the Simulation Period

System	RMSD *backbone* (nm)	RMSD ligands (nm)	RMSF (nm)
	150 ns	150 ns	
ALR2-APO	0.167 ± 0.025	-	0.315 ± 0.075
ALR2-M15	0.136 ± 0.016	0.058 ± 0.009	0.279 ± 0.083
ALR2-ZST	0.132 ± 0.014	0.072 ± 0.018	0.355 ± 0.133
ALR2-SDU18	0.155 ± 0.022	0.085 ± 0.019	0.491 ± 0.164
ALR2-SDT18	0.171 ± 0.024	0.095 ± 0.016	1.027 ± 0.435
ALR2-SDT12	0.135 ± 0.016	0.069 ± 0.014	0.462 ± 0.129

RMSF analysis assessed amino acid residue flexibility, showing that ALR2-SDT18 had the highest average RMSF (1.027 ± 0.435 nm), particularly in residues 18–80, 110–147, 159–230, and 260–316 (Table-3), indicating greater flexibility and reduced stability (Fig.-5). In contrast, the ALR2-APO system exhibited lower fluctuations.

Radius of gyration analysis assessed protein-ligand compactness, showing that all systems remained relatively stable, with RoG values between 1.920 and 1.940 nm during the final 10 ns of the simulation (Table-3, Fig.-5).

Table-3: Average RoG Values of Each System During the Last 10 ns of the Simulation

System	RoG (nm)
ALR2 - APO	1.932 ± 0.007
ALR2 – M15	1.925 ± 0.006
ALR2 - ZST	1.925 ± 0.005
ALR2 – SDU18	1.925 ± 0.004
ALR2 – SDT18	1.930 ± 0.006
ALR2 – SDT12	1.937 ± 0.005

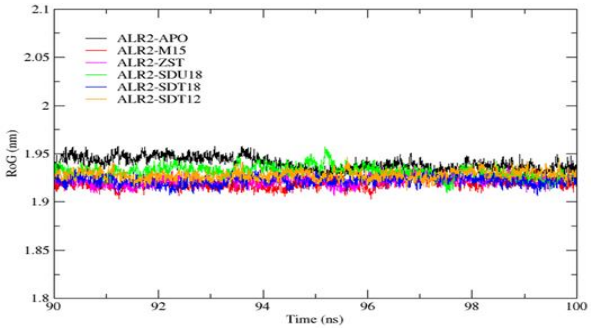

Fig.-5: Result of RoG Analysis

SASA analysis, which reflects protein surface exposure and stability, showed that ALR2-SDT12 had the highest values (entire enzyme: 13.697 ± 1.075 nm²; active site: 138.861 ± 2.576 nm²), indicating greater flexibility. In contrast, ALR2-M15 exhibited the most stable active site (9.168 ± 0.894 nm²), while ALR2-ZST showed the greatest overall enzyme stability (132.430 ± 2.534 nm²) (Fig.-6).

Table-4: Average SASA Values for the Active Site and the Entire Enzyme

System	SASA (nm^2)	
	Active site	Entire enzyme
ALR2 - APO	13.281 ± 1.314	136.231 ± 2.905
ALR2 – M15	9.168 ± 0.894	135.762 ± 3.131
ALR2 - ZST	13.484 ± 1.042	132.430 ± 2.534
ALR2 – SDU18	11.912 ± 1.042	132.717 ± 2.495
ALR2 – SDT18	9.872 ± 0.949	136.839 ± 3.024
ALR – SDT12	13.697 ± 1.075	138.861 ± 2.576

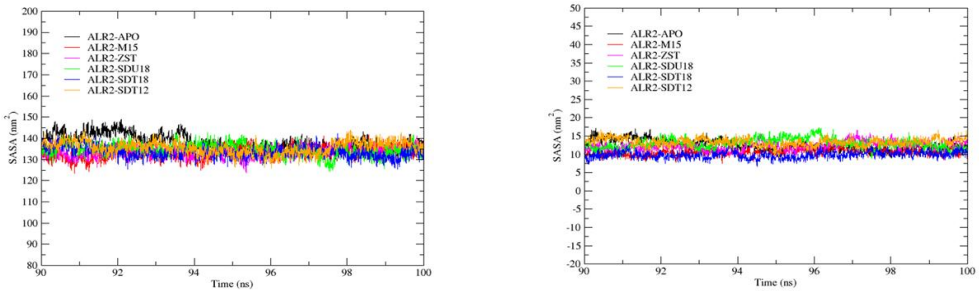

(a) (b)

Fig.-6: SASA Analysis at the Last 10 ns (a) at Active Site, (b) Entire Enzyme

Estimation of Binding Free Energy

The binding free energy (ΔG_bind), an important indicator of protein–ligand stability and affinity, was calculated using the MM-PBSA and MM-GBSA methods based on the final 10 ns of stable simulation trajectories. Energy contributions were calculated for gas-phase (ΔG_GB) and solvent-phase (ΔG_PB) components, including van der Waals and electrostatic interactions, with results summarized in Table-5.

Table-5: Predicted Binding Free Energy (Kcal/mol ± average standard error) using MMPBSA and MMGBSA Approaches

Energy component	ALR2-ZST	ALR2-SDU18	ALR2-SDT18	ALR2-SDT12
ΔE_{vdW}	-47,89 ± 0,19	-36,01 ± 0,20	-34,09 ± 0,18	-38,65 ± 0,21
ΔE_{ele}	-7,76 ± 0,59	4,19 ± 1,62	17,94 ± 0,84	6,12 ± 1,41
ΔG_{GBele}	27,47 ± 0,45	17,85 ± 1,48	-2,87 ± 0,75	16,51 ± 1,32
ΔG_{GBsolv}	21,35 ± 0,45	12,84 ± 1,48	-7,80 ± 0,75	11,51 ± 1,31
ΔG_{GBbind}	-34,31 ± 0,23	-18,97 ± 0,24	-23,94 ± 0,21	-21,02 ± 0,28
ΔG_{PBele}	24,21 ± 0,43	19,36 ± 1,49	0,62 ± 0,73	18,11 ± 1,35
ΔG_{PBsolv}	18,31 ± 0,43	14,21 ± 1,49	-4,98 ± 0,72	12,91 ± 1,34
ΔG_{PBbind}	-37,35 ± 0,29	-17,61 ± 0,37	-21,12 ± 0,28	-19,61 ± 0,38

As shown in Table-5, GB and PB binding free energy predictions were comparable. Van der Waals interactions contributed most to complex stability, while electrostatic energy was significant only for ALR2-ZST (-7.76 ± 0.59 kcal/mol). Solvent-phase contributions were generally minimal, except for ALR2-SDT18 (-7.80 ± 0.75 kcal/mol). ALR2-ZST showed the lowest ΔGGBbind and ΔGPBbind values (-34.31 ± 0.23 and -37.35 ± 0.29 kcal/mol), consistent with docking grid scores, although overall binding energies were similar across systems.

Analysis of Energy Decomposition

Energy decomposition analysis identified a few key residues contributing significantly to ligand-enzyme binding, with no residues showing unfavorable interactions. Energy decomposition analysis identified Trp21 and Leu301 as major contributors to binding across ALR2-ZST, ALR2-SDU18, ALR2-SDT18, and ALR2-SDT12. Additional stabilizing residues included His111 and Trp112 (ALR2-ZST), Lys22 (ALR2-SDT18), and Leu301 (ALR2-SDT12). Electrostatic interactions, alongside van der Waals forces, were key to complex stability, while solvation effects were minor.

Ligand – Enzyme Interaction

Ligand–protein interactions near the active site were analyzed over the last 10 ns of simulation, focusing on residues within 3.5 Å and an average angle >140°. Three interaction types—hydrogen bonding, van der Waals, and π-π stacking were observed. The ligand structures used in the analysis are shown in Fig.-7.

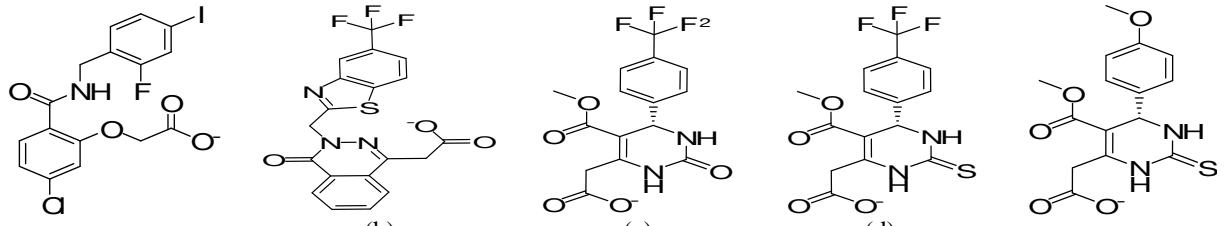

(a) (b) (c) (d) (e)

Fig.-7: Molecular Structure of the Tested Ligands: (a) M15; (b) ZST; (c) SDU18; (d) SDT18; (e) SDT12

Hydrogen-bond interactions between the ligand and protein during the final 10 ns of simulation are discussed followed. Each system formed approximately 3–4 hydrogen bonds, with the key residues varying by complex. In ALR2-M15 and ALR2-ZST, Tyr49, His111, and Trp112 were primary contributors, while Trp21, Lys22, and His111 dominated in ALR2-SDU18, ALR2-SDT18, and ALR2-SDT12. The candidate systems exhibited distinct binding poses and weaker hydrogen bonding than the reference complexes, with bonding fractions below 50%, indicating lower overall stability. Van der Waals and π-π stacking interactions within 3.5 Å of the active site (average distance 4 Å) influenced system stability, with higher interaction counts indicating greater stability. ALR2-M15 and ALR2-ZST showed

strong stability, supported by Tyr49 and His111 (van der Waals) and Trp112 (π-π stacking), with interaction fractions above 50%. In contrast, the candidate systems were less stable due to fewer interactions, although ALR2-SDU18 exhibited the highest stability among them, with π-π stacking and van der Waals interactions involving Trp112 (55.9%).

CONCLUSION

A library of 288 dihydropyrimidinone-based candidates was designed as potential ALR2 inhibitors, selected based on grid scores, docking poses, ADMET properties, and drug-likeness. Molecular dynamics simulations revealed that three compounds—2-(5-(methoxycarbonyl)-2-oxo-6-(4-(trifluoromethyl)phenyl)-1,2,3,6-tetrahydropyrimidin-4-yl)acetate, 2-(5-(methoxycar-bonyl)-2-thioxo-6-(4-(trifluoromethyl)phenyl)-1,2,3,6-tetrahydropyrimidin-4-yl)acetate, and 2-(5-(methoxycarbonyl)-6-(4-methoxyphenyl)-2-thioxo-1,2,3,6-tetrahydropyrimidin-4-yl)acetate—formed stable complexes and showed promising inhibitory activity, though zopolrestat was more potent. Trp21 and Trp112 were identified as key residues in the inhibitory mechanism, emphasising their relevance for future ALR2 inhibitor design.

ACKNOWLEDGMENTS

The authors acknowledge Universitas Airlangga for the research funding through Hibah Riset Mandat 2019 research scheme, grant no.1408/UN3/2019

CONFLICT OF INTERESTS

The authors declare that there is no conflict of interest.

AUTHOR CONTRIBUTIONS

The present work is related to *SDG-3: Good Health and Well Being*. All the authors contributed significantly to this manuscript, participated in reviewing/editing and approved the final draft for publication. The research profile of the authors can be verified from their ORCID ids, given below:

H. Suwito http://orchid.org/0000-0002-5844-067X
M.F.B. Darmawan http://orchid.org/0000-0003-1850-3768
K.U. Haq http://orchid.org/0000-0002-0584-5040
I. Siswanto http://orchid.org/0000-0001-9811-0977

Cite this article as: H. Suwito *et al.*, *Rasayan J. Chem.*, 19(3), 1331-1339(2026), https://doi.org/10.31788/RJC.2026.1939735

REFERENCES

1. C. Chalk, T.J. Benstead, F. Moore, *Cochrane Database of Systematic Review*. **4**, CD004572 (2007), http://dx.doi.org/10.1002/14651858.CD004572.pub2
2. International Diabetes Federation, Diabetes Atlas, 11th Ed., diabetes atlas.org, New York, 8-10 (2025).
3. J. Dowarah, V.P. Singh, *Bioorganic and Medicinal Chemistry*, **1:28(5)**, 115263(2020). http://dx.doi.org/10.1016/j.bmc.2019.115263
4. P. Alexiou, K. Pegklidou, M. Chatzopoulou, I. Nicolaou, V.J. Demopoulos, *Current Medicinal Chemistry*, **16(6)**, 734(2009), http://dx.doi.org/ 10.2174/092986709787458362
5. M. Digiacomo, S. Sartini, G. Nesi, S. Sestito, V. Coviello, C. La Motta, S. Rapposelli, *The Open Medicinal Chemistry Journal*, 2017, **11**, 9(2017), http://dx.doi.org/10.2174/-1874104501711010009
6. M.A. Pfeifer, M.P. Schumer, D.A. Gelber, *Diabetes*, 1997, **46(2)**, S82(1997), http://dx.doi.org/10.2337/diab.46.2.S82
7. C.A. Thorne, C.G. Angus, J.C. Lim, P.J. Donaldson, *International Journal of Molecular Sciences*, **25(16)**, 9042(2024), https://doi.org/10.3390/ijms25169042
8. A-I. Dănilă, L.A. Ghenciu, E.R. Stoicescu, S.L. Bolintineanu, R. Iacob, M-A. Săndesc, A.C. Faur, *Biomedicines*, **12**, 747(0204), https://doi.org/10.3390/biomedicines-12040747

9. M Stefek, MS Prnova, J Ballekova, M Majekova, 2016, Cemtirestat, *International Journal of Advances in Science Engineering and Technology*, **4(3)**, 41(2016).
10. H. Suwito, N. Kurnyawaty, K.U. Haq, R. Ramadhan, A. Abdulloh, H.D. Hardiyanti, P. Phuwapraisirisan, *Rasayan Journal of Chemistry*, 2023, **16(1)**, 147, https://doi.org/10.31788/RJC.2023.1618025
11. P. Kirsch, A.M. Hartman, A.K.H. Hirsch, E. Empting, *Molecules*, **24(23)**: 4309(2019), https://doi.org/10.3390/molecules24234309
12. J. Fanfrlik, M. Kolar, D. Kamlar, D. Hurny, F.X. Ruiz, A. Cousido-Siah, A. Mitschler, J. Rezac, E. Munusamy, M. Lepsik, P. Matejicek, J. Vesely, A. Podjarny, H. Hobza, *ACS Chemical Biology Journal*, **8**, 2484(2013), https://doi.org/10.1021/cb400526n
13. M.J. Frisch, G.W. Trucks, H.B. Schlegel, G.E. Scuseria, M.A. Robb, et al., Gaussian 16, Revision C.01, 2016, Gaussian Inc., Wallingford CT.
14. J. Wang, W. Wang, P.A. Kollman, D.A. Case, *Journal Chemical Information and Computer Sciences,* **41(6)**, 1486(2001).
15. E.F. Pettersen, T.D. Goddard, C.C. Huang, G.S. Couch, D.M. Greenblatt, E.C. Meng, T.E. Ferrin, *Journal of Computational Chemistry*, **25**, 1605(2004),https://doi.org/-10.1002/jcc.20084
16. J.A. Maier, C. Martinez, K. Kasavajhala, L. Wickstrom, K.E. Hauser, C. Simmerling, *Journal of Chemical Theory and Computation*, **11**, 3696(2015), https://doi.org/10.1021/acs.jctc.5b00255
17. R.L. DesJarlais, G.L. Seibel, I.D. Kuntz, R.P. Sheridan, R. Venkataraghavan, R.J. Scott-Dixon, 1988, *Journal of Medicinal Chemistry*, **31**, 722(1988), https://doi.org/-10.1021/jm00399a006
18. E.C. Meng, B.K. Shoichet, I.D. Kuntz, *Journal of Computational Chemistry*, **13**, 505(1992), https://doi.org/10.1002/jcc.540130412
19. W.J. Allen, T.E. Balius, S. Mukherjee, S.R. Brozell, D.T. Moustakas, P.T. Lang, D.A. Case, I.D. Kuntz, R.C. Rizzo, *Journal of Computational Chemistry*, **36**, 1132(2015), https://doi.org/10.1002/jcc.23905
20. A. Daina, O. Michielin, V. Zoete, *Scientific Report*, **7**, 42717(2017), https://doi.org/10.1038/srep42717
21. M.T. Martin, User's Guide for T. E. S. T. (Toxicity Estimation Software Tool Version 5.1), U.S. Environmental Protection Agency, Washington, D.C., 2020.
22. L.M. Castro-González, J.R. Alvarez-Idaboy, A. Galano, *ACS Omega*, **5**, 9566(2020), https://doi.org/10.1021/acsomega.0c00898
23. D.A. Case, H.M. Aktulga, K. Belfon, I.Y. Ben-Shalom, J.T. Berryman, S.R. Brozell, D.S. Cerutti, T.E. Cheatham III, G.A. Cisneros, V.W.D. Cruzeiro, T.A .Darden, R.E. Duke, G. Giambasu, *et al.*, *Amber - Reference Manual*, 2022, University of California, San Fransisco, 2022.
24. S. Genheden, U. Ryde, *Expert Opinion Drug Discovery*, **10**, 449(2015),https://doi.org 10.1517/17460441.2015.1032936
25. X. Hou, D. Rooklin, D. Yang, X. Liang, K. Li, J. Lu, C. Wang, P. Xiao, Y. Zhang, J. Sun, H. Fang, *Journal of Chemical Information and Modeling*, **58**, 2331(2019), https://doi.org/10.1021/acs.jcim.8b00548
26. P.A. Greenidge, C. Kramer, J.C. Mozziconacci, R.M. Wolf, *Journal of Chemical Information and Modeling*, **53**, 201(2013), https://doi.org/10.1021/ci300425v
27. B. Mohammadi, F..K Behbahani, *Molecular Diversity*, **22**, 405(2018), https://doi.org/10.1007/s11030-017-9806
28. C.A. Lipinski, F. Lombardo, B.W. Dominy, P.J. Feeney, *Advanced Drug Delivery Reviews*, **64**, 4(20120, https://doi.org/10.1016/j.addr.2012.09.019
29. S.A. Ali, M.I. Hassan, A. Islam, F. Ahmad, *Current Protein & Peptide Science*, **15(5)**, 456(2014), https://doi.org/10.2174/1389203715666140327114232
30. C.D. Geierhaas, A.A. Nickson, K. Lindorff-Larsen, J. Clarke, M. Vendruscolo, *Protein Science*, **16**, 125(2007), https://doi.org/10.1110/ps.062383807
31. H. Hata, D.P. Tran, M.M. Sobeh, A. Kitao, *Biophysics and Physicobiology*, **18**, 305 (2021), https://doi.org/10.2142/biophysico.bppb-v18.037
32. T. Tuccinardi, *Expert Opinion Drug Discovery*, **16(11)**, 1233(2021), https://doi.org/10.1080/17460441.2021.1942836

[RJC-9735/2026]